

DNA Origami-Directed Self-Assembly of Gold Nanospheres for Plasmonic Metasurfaces

Christoph Sikeler, Franziska Haslinger, Irina V. Martynenko, and Tim Liedl*

Plasmonic nanostructures are frequently utilized to create metasurfaces with a large variety of optical effects. Control over shape and positioning of the nanostructures is key to the function of such plasmonic metasurfaces. Next to lithographic means, directed self-assembly is a viable route to create plasmonic structures on surfaces with the necessary precision. Here, a combined approach of DNA origami self-assembly and electron beam lithography is presented for determinate positioning of gold nanospheres on a SiO₂ surface. First, DNA origami structures bind to the electron beam-patterned substrate and subsequently, gold nanoparticles attach to a defined binding site on the DNA origami structure via DNA hybridization. A sol-gel reaction is then used to grow a silica layer around the DNA, thereby increasing the stability of the self-assembled metasurface. A mean yield of 74% of single gold nanospheres is achieved located at the determinate positions with a spatial position accuracy of 9 nm. Gold nanosphere dimers and trimers are achieved with a rate of 65% and 60%, respectively. The applicability of this structuring method is demonstrated by the fabrication of metasurfaces whose optical response can be tuned by the polarization of the incoming and the scattered light.

1. Introduction

Metasurfaces contain sub-wavelength features to tailor the phase and amplitude of electromagnetic waves in a defined way. Applications range from imaging with flat lenses^[1] over wavefront control for beam shaping^[2] to nonlinear optical effects.^[3] Usually, metasurfaces gain their optical properties through designed variation of the refractive index. This variation can be achieved with plasmonic features precisely arranged depending on the desired purpose of the metasurface. Such small features are usually

fabricated via electron beam lithography (EBL) or directed self-assembly (DSA).^[4–7] Among the self-assembly approaches, DNA origami has proven to be a powerful and reliable tool.^[8–14]

The DNA origami method exploits the sequence specificity of Watson-Crick base-pairing to fold a long single-stranded DNA (ssDNA) strand (scaffold strand) together with roughly 200 short oligonucleotides (staple strands) into 2D and 3D nanostructures.^[15–17] Each of the staple strands can be chemically modified or the sequence can be extended from the surface of the DNA structure and thus be used as an anchor to site-specifically attach functional moieties.^[18] A resolution of ≈ 1 nm can be achieved for gold nanospheres (AuNS).^[19] Suitable functional molecules include fluorescent dyes,^[20] proteins,^[13] quantum dots,^[21] or plasmonic nanoparticles.^[22]

A 2D DNA origami structure can have an overall size well above 80 nm.^[9]

Therefore, EBL is suitable to fabricate binding sites for DNA origami structures on various surfaces.^[23] Precise positioning of DNA origami on SiO₂ surfaces has been demonstrated with a yield of up to 94%.^[24] By creating DNA origami structures with a C₁ symmetry, Gopinath et al. reduced the rotational degree of freedom of each DNA origami structure on a binding site to $\approx 3^\circ$.^[12] This enables the combination of EBL and DNA origami as DSA to fully control the position and the orientation of each DNA origami structure on a surface.

Several groups have developed protocols to use DNA origami structures as lithography masks to fabricate metallic and dielectric nanostructures.^[4–6,8,10,11,25,26] As an example, the change of surface wetting of SiO₂ beneath a DNA origami structure compared to air during HF vapor-phase etching can be used to transfer the shape of the DNA template on the SiO₂ surface either as negative or positive tone template depending on the temperature and the humidity.^[5,10] Further HBr/O₂ plasma etching can be utilized to use the thus created SiO₂ mask for subsequent etching of the bare Si substrate.^[8] Alternatively, the DNA origami structures can be placed on a Si surface after which SiO₂ can be selectively grown on the bare Si substrate. Consequently, the SiO₂ layer has DNA origami-shaped holes. Following subsequent etching and metal deposition steps the shape of the original DNA origami structure is recovered in a metal nanostructure.^[4]

C. Sikeler, F. Haslinger, I. V. Martynenko, T. Liedl
Ludwig-Maximilians-Universität
Geschwister-Scholl-Platz 1, 80539 München, Germany
E-mail: tim.liedl@physik.lmu.de

The ORCID identification number(s) for the author(s) of this article can be found under <https://doi.org/10.1002/adfm.202404766>

© 2024 The Authors. Advanced Functional Materials published by Wiley-VCH GmbH. This is an open access article under the terms of the Creative Commons Attribution-NonCommercial-NoDerivs License, which permits use and distribution in any medium, provided the original work is properly cited, the use is non-commercial and no modifications or adaptations are made.

DOI: 10.1002/adfm.202404766

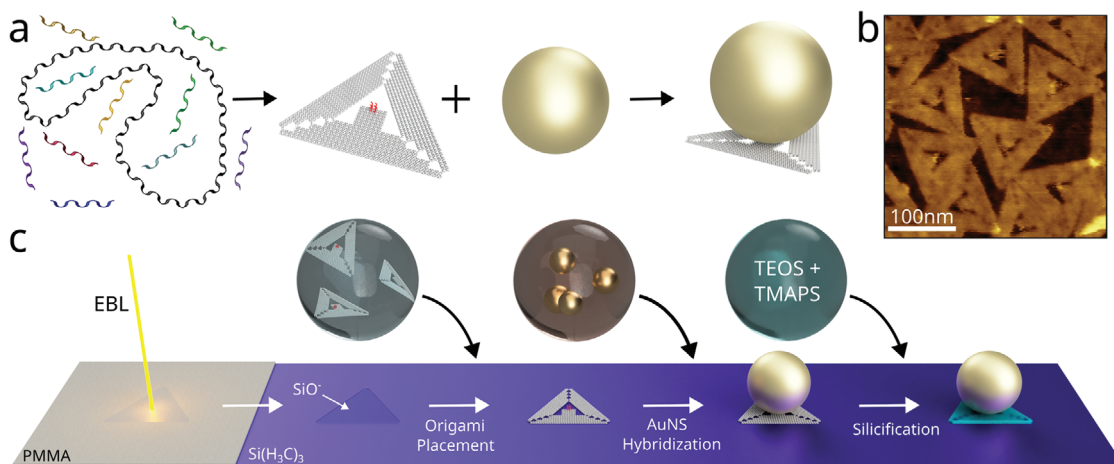


Figure 1. a) A DNA origami structure self-assembles during thermal annealing. An anchor site for a nanoparticle is indicated in red in the center of the triangle. The plasmonic nanoparticles are conjugated via a complementary DNA sequence to the anchor site. b) Liquid atomic force microscopy image of DNA origami triangles. c) Scheme of AuNS placement: i) EBL is used to pattern triangular shapes in PMMA; ii) O_2 plasma cleaning results in hydrophilic triangular areas on a hydrophobic background; iii) DNA origami structures attach to the hydrophilic areas via salt bridges; iv) AuNSs attach to the center of the DNA origami structure; v) in a sol-gel reaction a silicon layer is grown around the product.

A different approach of DSA with DNA origami exploits the capability of DNA origami as a precise anchor point for guest molecules.^[9,13,14] For example, Gopinath et al. controlled the spatial position of a DNA origami structure inside a nanocavity.^[14] Three ssDNA regions in the center of the DNA origami structure are used to capture one Cy5 molecule to each anchor point. Therefore, enabling them to precisely control the position and amount of fluorescent molecules in the nanocavity. Hung et al. presented a method in which AuNSs with a diameter of 5 nm attach to each tip of a triangular DNA origami structure and subsequently immobilize on a surface.^[9] The hybridization of DNA origami and AuNSs was performed in solution and is followed by precise positioning of the so-formed structures via EBL on a SiO_2 substrate. Hence, enabling them to pattern the surface with in liquid fabricated DNA origami-AuNS complexes creating a landscape with sub-10 nm plasmonic features.

Here, we demonstrate the fabrication of a plasmonic metasurface fabricated by DNA origami-DSA of AuNSs. We achieved a yield as high as 74% of placement of single AuNSs of 100 nm diameter with a precision of 9 nm. We used a sol-gel reaction to grow a silica shell around the dsDNA to increase the structural rigidity of the fabricated metasurfaces which enabled air-drying of the nanostructures. We demonstrate dynamic tunable coloration of our metasurfaces consisting of arrays of single AuNSs, AuNS dimers, and AuNS trimers. The AuNS dimers and trimers were fabricated with a yield of 65% and 60%, respectively. Finally, polarization-dependent scattering cross-sections of our nanostructures were utilized to create an image that shows different letters depending on the selected polarization.^[27]

2. Experimental Section

2.1. DNA Origami

The triangular DNA origami structure was designed with cadnano.^[17] The DNA origami structure was formed of three

trapezoids forming an equilateral triangle with a side length of 127 nm. The empty equilateral triangle in the center of the structure is filled with a rectangular extension from one of the trapezoids, see **Figure 1a**. The 242 staple strands used for the folding were purchased from IDT Technologies. The scaffold strands (p8064) were derived from M13 phages replicated in *Escherichia Coli*.^[15] A mixture of 100 μ L containing 10 nm scaffold, 100 nm of each staple strand, 8 mm $MgCl_2$, 10 mm TRIS-HCl, and 1 mm EDTA at a pH of 8 was mixed and incubated in a thermal cycler (Tetrad 2 Peltier thermal cycler, Bio-Rad). The temperature was kept at 65 $^{\circ}C$ for 15 min before lowering it from 54 $^{\circ}C$ to 49 $^{\circ}C$ by 1 $^{\circ}C$ every 30 min.

2.2. DNA Origami Purification: Rate-Zonal Centrifugation

The purification of the DNA origami structures from excess staple strands was performed similarly to ref. [28] The glycerol gradient consisted of three layers with a 50/50, 30/70, and a 10/90 ratio of glycerol to TRIS-Acetate-EDTA buffer (TAE buffer) containing 11 mm $MgCl_2$. Each layer had a volume of 300 μ L. SYBR gold purchased from Thermo Fischer Scientific was added to the DNA origami mixture prior to pipetting the mixture on top of the gradient. The sample was centrifuged for 1 h at 100,000 rcf in a Beckman Coulter Optima MAX-XP centrifuge. A self-made illumination device, built from an excitation LED and a high pass filter, was used to visualize the staple and the DNA origami band. The supernatant was removed until the DNA origami band became accessible. Subsequently, this DNA origami layer could be extracted. The concentration of DNA origami structures was determined with a NanoDrop ND-1000 spectrophotometer (Thermo Scientific). Structural integrity of the DNA origami triangles was confirmed by gel electrophoresis and liquid atomic force microscopy (Bruker Nanoscope 2).

2.3. Gold Nanospheres

Attachment of AuNSs to the center of the DNA origami triangles was done by DNA hybridization. To this end, the surface of the AuNSs must be functionalized with ssDNA which is complementary to the sequence of the ssDNA extensions of the anchor point. In the experiment AuNSs with a diameter of 100 nm purchased from BBI were used and their surface was modified with thiolated ssDNA (T19) ordered from Biomers. The T19 had a sequence of 19 consecutive thymine bases, complementary to the ssDNA extensions at the anchor point. The six ssDNA extensions at the center of the DNA origami triangle had a sequence of 15 consecutive adenine bases. The surface modification of the AuNSs with the thiolated DNA was done by the freeze-thaw method. Two times 2 mL of the AuNS solution were centrifuged at 2500 rcf for 5 min. 1.5 mL of the supernatant was removed of both tubes without disturbing the particles. The content of both tubes was mixed and 100 μ L of 100 μ M T19 was added to the particles before mixing and freezing the solution at -70 °C. The particles were thawed at room temperature. The functionalized AuNSs were purified from unbound ssDNA by centrifugation. To this end, the particles were centrifuged at 2500 rcf for 5 min. The supernatant was removed and replaced by ddH₂O. The process was repeated five times but with placement buffer (PB; 5 mm TRIS at pH 8.5) at the fifth time. Filtration with a 0.22 μ m filter unit (Spin-X Centrifuge Tube Filter, Costar) reduced AuNS clusters in the later experiment.

2.4. Precise Placement of AuNSs on SiO₂ Surfaces via DNA Origami

Placement of AuNSs on SiO₂ surfaces was done via a two-step process following the protocols presented by Martynenko et al.^[29] and subsequent AuNS attachment. First, the SiO₂ substrates were prepared and patterned with 120 nm triangular binding sites precisely following the protocol presented in Ref. [29] with all materials and instruments identical. DNA origami placement on the prepared SiO₂ surfaces followed the protocol of Gopinath et al.^[24] with small variations. The concentration of DNA origami structures during the incubation was set to 300 pm in PB containing 35 mm MgCl₂ with a total volume of 60 μ L. After the 1 h incubation at 30 °C in an incubator (TECO, Selutec) the surface was washed 4x with 100 μ L PB containing 35 mm MgCl₂ and 8x with 100 μ L of the 0.5% washing buffer (0.5% WB; 5 mm TRIS at pH 8.5, 35 mm MgCl₂ and 0.5% Tween20). Every washing step was performed by adding the indicated volume pipetting up and down 2–3 times and removing the indicated volume. Subsequently, the surface is incubated for 30 min at room temperature before another washing step with 3x 100 μ L of 0.1% washing buffer (0.1% WB; 5 mm TRIS at pH 8.5, 35 mm MgCl₂ and 0.1% Tween20). 50 μ L AuNSs at an OD of 0.15 in PB containing 35 mm MgCl₂ were added to the droplet. The sample was incubated over night at 35 °C inside a closed petri dish with a small piece of moistened kimwipe. Next, the surface was washed for 8x with 100 μ L of 0.1% WB and incubated for 30 min at room temperature. Before proceeding with either drying the sample or silicification, the surface was washed multiple times with 100 μ L PB containing 35 mm

MgCl₂ until a droplet formed on the hydrophobic surface. The sample was silicified according to the protocol of Liu et al.^[30] with a ratio of TMAPS:TEOS of 2%. After silicification the sample was dipped in ddH₂O for 40 s and for 10 s in isopropanol to clean the substrate from the residual chemicals. The remaining isopropanol evaporated and left a dry surface with the designed pattern.

2.5. Characterization Techniques

The darkfield microscopy set-up is an Olympus BX51 with a 100x objective (Olympus MPLFLN100XBD). The sample was illuminated from above. A rotatable linear polarization filter was located between the objective and the CCD camera (Kiralux, Thorlabs) to select certain polarization states. Spectra were acquired with the same optical set-up but with a Acton SpectraPro SP-2300 from Princeton Instruments instead of the camera.

The EBL of the wafers was done with a Raith e-Line device. The patterning was done with a beam energy and current of 20 keV, a dosage of 400 $\frac{\mu C}{cm^2}$ and a 20 μ m aperture.

SEM images were acquired with a LEO FE-REM 982 Gemini with a beam energy of 5 keV. No further treatment of the sample for the imaging was needed.

Liquid AFM (Nanowizard Ultraspeed 2, JPK) images were acquired in PB on SiO₂ surfaces. 60 μ L of 1 nm DNA origami structures in PB containing 35 mm MgCl₂ were incubated for 3 min on the surface prior to adding 3 mL PB containing 35 mm MgCl₂. The images were acquired in peak-force tapping mode with a AC40TS tip.

2.6. Analysis

The artificial intelligence (AI) python package cellpose^[31] was used to recognize the AuNSs on the SEM images. An additional python algorithm was used to segment the SEM image into single lattice sites. For each of those segments a classification of the lattice site was performed according to the amount of AuNSs recognized by the AI. Furthermore, the python library openCV was used to determine the center of each AuNS detected by the AI. The nearest neighbor distribution was then calculated from the centers of the AuNS. The distances between the centers of all single AuNSs were calculated and used for the distribution of nearest neighbors if the distance was within the range of 600 to 800 nm. For all lattice sites that were classified as two AuNSs the unit vector connecting the centers of the two AuNSs was determined. Subsequently, the angle between the horizontal lattice vector and the unit vector was calculated as the dimer orientation. Also for all lattice sites classified as three AuNSs the center of each sphere was determined. The center with the lowest y-coordinate was determined as the center of the top AuNS, the center with the highest x-coordinate was determined as the center of the most right AuNS and the center of the bottom AuNS was determined as the remaining center. From the three centers the unit vectors connecting the particles could be calculated and subsequently the orientation and opening angle of the AuNS trimer structure.

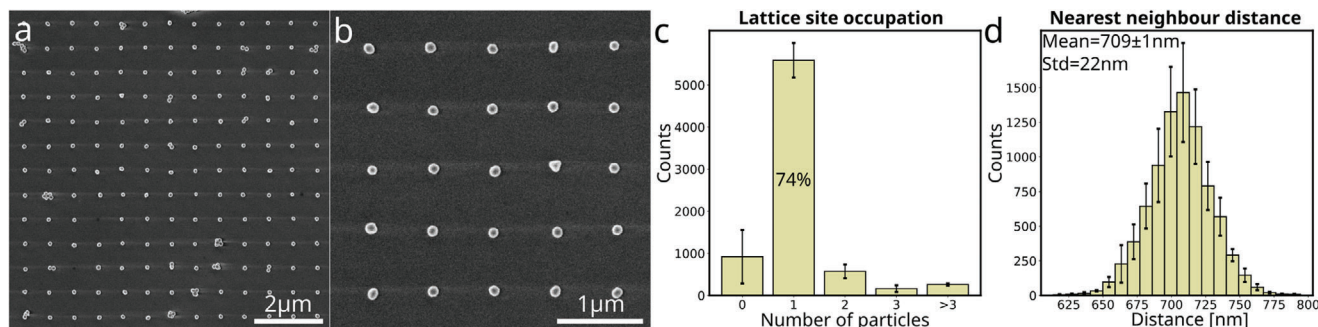


Figure 2. a,b) Large field of view and zoom-in SEM image of a square lattice of single AuNSs with a lattice constant of 700 nm. c) Histogram of lattice occupancy of 7500 lattice sites for a single particle lattice. d) Distribution of the nearest neighbor distance for a square lattice of single AuNSs with a lattice constant of 700 nm. The measured mean distance is 709 nm which differs from the designed lattice constant by only 9 nm.

2.7. Reproducibility

For all statistics four individual repetitions of the experiment were performed. Each experiment contained three identical patterns, each lattices with 50×50 spots. Hence, the data shown in the histograms results from four independent measurements each containing 7500 lattice sites. In the scope of this work a total of 90000 lattice sites have been investigated, 30000 each for the single AuNS, dimer and trimer lattice.

3. Results and Discussion

The protocol of Gopinath et al.^[24] with slight variations was followed to site-specifically attach the DNA origami structures to the SiO₂ surface. We utilized a monolayer triangular DNA origami structure similar to the structure published by Ruthemund.^[16] This structure has been used for a wide variety of purposes, including EBL-assisted placement of DNA origami structures. Due to its C₃ symmetry, the triangular DNA origami structure can attach to a triangular pattern in three different orientations. Only the center of the DNA origami structure stays at the same position independent of the DNA origami orientation. Since the original design of the equilateral triangle has a triangular hole in the center, we changed the design by including a 21.1 × 17.5 nm rectangle in the center to address this position as an anchor point for plasmonic nanoparticles. A schematic of the structure can be seen in Figure 1a and an atomic force microscopy image in Figure 1b. The schematic also shows the ssDNAs in the center forming the anchor position for plasmonic nanoparticles.

In order to attach to this anchor position the surface of the AuNSs is modified with a complementary DNA sequence. In our experiment, we used AuNSs with a diameter of 100 nm and modified their surface with T19. The AuNSs-bound ssDNAs hybridized with the ssDNAs of the DNA origami anchor point and thus connected the AuNS with the center of the DNA origami structure. Subsequently, a silica shell was grown around the ds-DNA in a sol-gel reaction which increased the rigidity of the DNA origami-AuNS complex. An illustration of the entire process can be found in Figure 1c.

First, we investigated the efficiency of AuNSs placement on our SiO₂ substrates. Therefore, we patterned a square lattice with a single AuNS at each lattice site. Each lattice side is categorized into one of five groups; empty site, single AuNS, AuNS dimer,

AuNS trimer, or AuNS cluster. SEM images of the lattice are shown in Figure 2a, b. The histogram corresponding to the classification is shown in Figure 2c. Overall, 74% of the lattice sites were occupied by exactly one AuNS, 12% were empty and 13% had more than one AuNS. Only a few particles (<< 1%) were observed to be randomly located on non-patterned areas of the surface.

To determine the spatial accuracy of our positioning method we compared the designed lattice constant of 700 nm with the mean nearest neighbor distance between the AuNSs. Only particles within a range of 600–800 nm were considered to be nearest neighbors. SEM images are used to determine the distance between AuNSs after following our placement protocol. A distribution of the nearest neighbor distances is plotted in Figure 2d. The mean distance is 709 nm which is only 9 nm or 1.3% larger than intended. The standard deviation for the mean distance is 22 nm. These mismatches may result from one of the following reasons or a combination thereof: i) error of the measurement technique or remaining error after calibration ii) the phase transition from liquid to dry induces enough force to break the bond between the DNA origami structure and the AuNS; iii) after attaching to a binding site, the DNA origami triangles move during subsequent steps of the placement protocol. However, the accuracy achieved is higher than that of other methods for colloidal particle placement like nanoparticle printing with <100 nm^[32] or laser printing with a precision of 50 nm.^[33]

Next, we investigated the deterministic placement of AuNSs in close proximity to each other. We fabricated a square lattice of AuNS dimer with a lattice constant of 700 nm. Figure 3a,b shows SEM images of the lattice with AuNS dimers oriented diagonally ascending and descending, respectively. A histogram of the lattice site occupation is depicted in Figure 3c. 65% of the lattice sites were occupied by two AuNSs, 16% by less than two AuNSs (3% empty, 13% single AuNS) and 20% by more than two AuNSs (12% three AuNSs, 8% more than three AuNSs).

The orientation of the AuNS dimers was designed to be diagonally ascending for 50% of the lattice sites and diagonally descending for the other 50%. A histogram of the angle between the long axis of the AuNS dimer and the horizontal lattice axis is shown in Figure 3d. The two peaks with a mean at 40° and 140° compared to the intended 45° and 135° indicate good control over the orientation of the AuNS dimer axis. In comparison, color laser printing provides an angular control of ± 16°.^[34] The

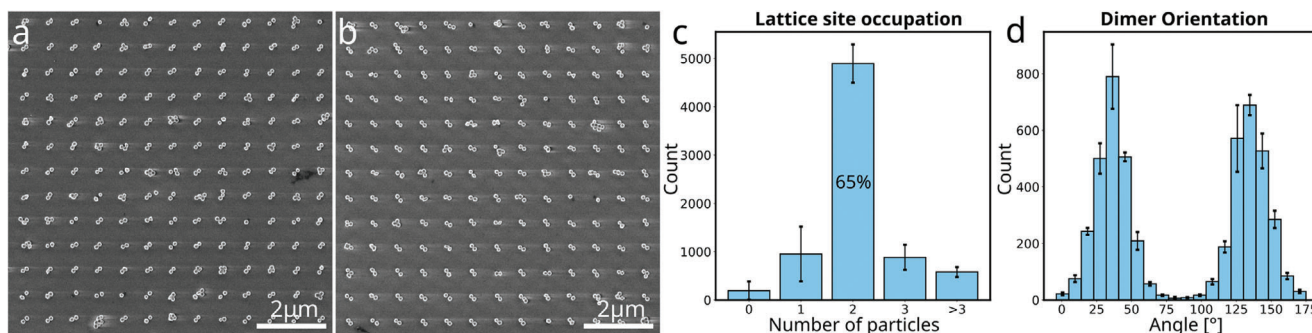


Figure 3. a, b) SEM image of a square lattice of AuNS dimers oriented diagonally ascending and descending, respectively. The lattice constant is 700 nm with a center to center distance of 102 nm between the two AuNSs. c) Histogram of site occupancy for a lattice with two AuNSs per lattice site. 7500 lattice sites were analyzed. d) Histogram of the angle between the long axis of the dimer and the horizontal lattice axis. The two peaks arise from the two different orientations, diagonally ascending and descending.

control over the exact gap size in our experiments was difficult to determine. The intended center-to-center distance between the two AuNSs of a dimer was 102 nm, resulting in an expected gap size of 2 nm, which is far below our SEM resolution. The spectral response of our samples, however, indicates a gap size between particle surfaces below 4 nm (Figure 47, Supporting Information). Note that also the size distribution and shape variations of the AuNSs, their DNA coating as well as the silica growth influences the effective particle-to-particle distance.

Another square lattice with three AuNSs per binding site is shown in Figure 4a and yielded 60% of AuNS trimers on the lattice sites. A full statistic of the lattice site classifications can be found in Figure 4b. Zero AuNSs were found in 1%, one AuNS in 3%, two AuNSs in 13%, and more than three AuNSs in 24%. Both for the dimer and the trimer case we observed higher binding yields compared to the yield expected from the single AuNS placement: $(74\%)^2 = 55\%$ and $(74\%)^3 = 41\%$, respectively. Therefore, we conclude that the AuNSs are not obstructing the binding of the second AuNSs but rather promote the binding of additional particles.

The designed arrangement of the three AuNSs is an arrow pointing right. The angle between the center-to-center connections of the top and the bottom AuNSs with the right-most AuNS is defined here as the opening angle. The orientation of the trimer

is determined by the angle between the center-to-center connection of the top AuNS with the bottom AuNS and the horizontal lattice vector. Both, the orientation angle and the opening angle are designed to be 90° . Figure 4c shows the histogram of the orientation of the lattice sites with three AuNSs. The mean angle is 85° proving again a good control over the rotational degree of freedom. However, Figure 4d presents a histogram of the opening angle of the lattice sites with three AuNSs and here the mean opening angle of 74° clearly differs from the intended angle of 90° . This could arise from capillary forces pulling the AuNSs together during the drying process. Increasing the strength of the connection between the DNA origami structure and the SiO_2 surface or increasing the rigidity of the DNA origami-AuNS complex might help to overcome this problem.

To demonstrate the capabilities of our method, we investigated the color response of single AuNSs, AuNS dimers oriented diagonally ascending, AuNS dimers oriented diagonally descending and AuNS trimers. An SEM image of the different AuNS configurations is shown in Figure 5a. Additionally, the scattering spectra for such a structure with a polarization diagonally descending (dark) and diagonally ascending (light) are plotted as well as respective dark-field images are shown. The spectra and the darkfield images matching demonstrates that the single AuNS appears green and the AuNS trimer red under both polarization

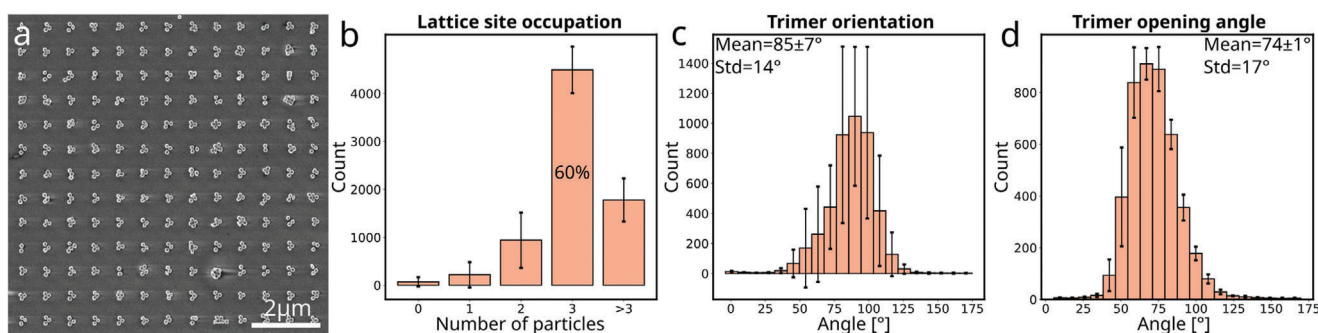


Figure 4. a) SEM image of a square lattice of AuNS trimers with a lattice constant of 700 nm. The trimer has the geometry of the tip of an arrow pointing right. b) Histogram of site occupancy for AuNS trimer placement. The number of analyzed lattice sites is 7500. c) Histogram of the orientation of the trimer structure. The angle is defined by the angle between the center-to-center connection of the top AuNS with the bottom AuNS and the horizontal lattice axis. The expected orientation would be 90° . d) Histogram of the trimer opening angle. The opening angle is defined as the angle between the center-to-center connection of the top and bottom AuNS with the most right AuNS. The designed opening angle is 90° .

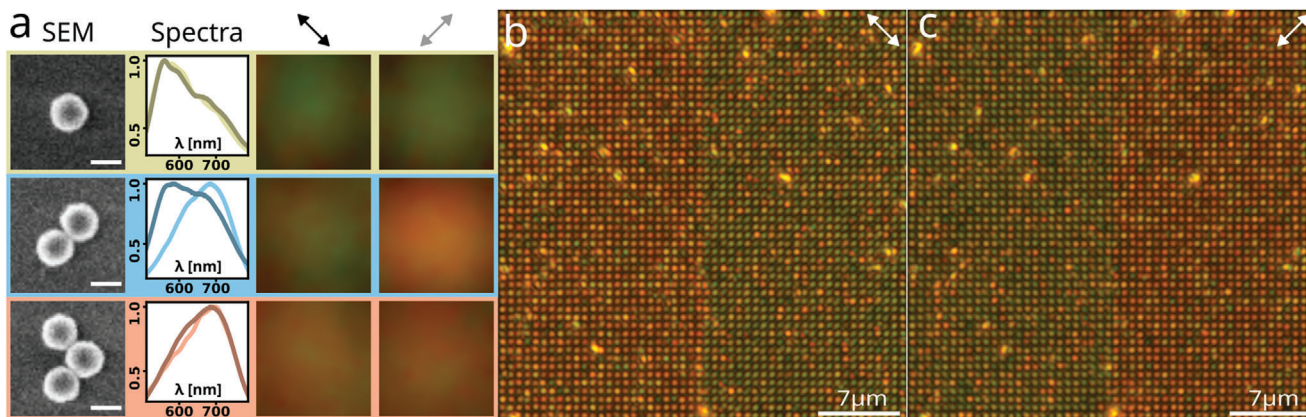


Figure 5. a) SEM images of a single AuNS, an AuNS dimer and an AuNS trimer. The scale bar is 100 nm. Experimentally acquired spectra of the respective lattices with a polarization direction diagonally descending (dark) and diagonally ascending (light). The dark-field images show representing optical responses of the AuNS configurations. b, c) shows dark-field images of a 50×50 AuNS dimer lattice. The 25 columns on the left (right) are oriented diagonally descending (ascending). In (b) the polarization is oriented diagonally descending whereas in (c) the polarization is oriented diagonally ascending.

states. The AuNS dimer changes its color from green to red depending on the angle between the long axis of the AuNS dimer and the polarization direction. For a polarization perpendicular to the axis of the dimer it appears green. For polarization along the axis, the AuNS dimer appears red. To illustrate the power of such an optical switch we fabricated a square lattice with a lattice constant 700 nm containing AuNS dimers on each lattice site. On the left half of the lattice the dimer is oriented diagonally descending whereas the dimers on the right half are oriented diagonally ascending. Figure 5b,c shows dark-field images of this lattice for diagonally descending and diagonally ascending polarization, respectively. A switch from green to red and vice versa is clearly

visible for almost all of the lattice sites. Histograms of the R, G, and B, values of all lattice sites can be found in Figures S44, S45, and S46 (Supporting Information). Shifts for the R and G values are visible whereas the B values do not change significantly.

By using single AuNSs, AuNS dimers in diagonally descending and ascending orientation and AuNS trimers, one obtains a full set of polarization-dependent pixels, as shown in Figure 5a. These three different structures can be used as pixels to create two red images on a green background. Depending on the selected orientation of the linear polarization filter, one of the two images is visible. We arranged the four different pixel in a square lattice in such a way that one can read LMU

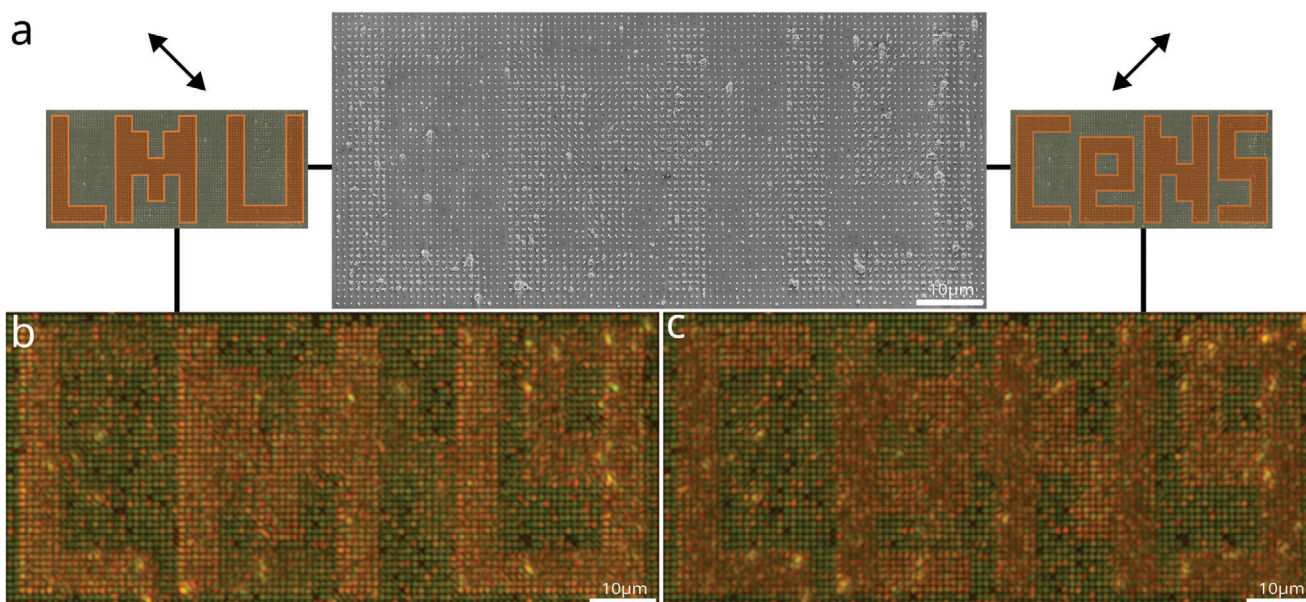


Figure 6. a) SEM image of a square lattice with lattice constant of 500 nm. By design, each lattice site should be occupied by either a single AuNS, a AuNS dimer diagonally descending or ascending or a AuNS trimer. The different motives are arranged on the lattice in a way that the meta surface displays either the LMU logo or the CeNS logo depending on the polarization of light. b) The meta surface under diagonally descending polarization in darkfield illumination. c) The meta surface under diagonally ascending polarization in darkfield illumination.

(Ludwig–Maximilians-Universität) for diagonally descending polarization and CeNS (Center for NanoScience) for diagonally ascending polarization. An SEM image of the meta-surface is shown in **Figure 6a** with indications for the intended color response under the two polarization directions. **Figure 6b,c** show the respective dark-field images for a polarization diagonally descending and ascending, respectively. The intended optical switch between the two polarization states is evident.

4. Conclusion

In conclusion, we have demonstrated a method combining DNA origami and EBL to fabricate optical nanostructures on SiO₂ surfaces from colloidal particles. While our approach focuses on spherical gold nanoparticles, future applications could require a combination of nanoparticles of different materials and various shapes. As any single DNA origami structure can carry multiple anchor sites, each with a different sequence enabling specific attachment of particles to those positions, multiple nanoparticles that are small compared to the size of the DNA origami structure could be positioned on a single DNA origami structure. If the size of the particles exceeds the size of the DNA origami structure, multiple DNA origami structures are necessary to resemble such a desired geometry. To this end, various DNA origami structures would need to attach to the surface in a specific manner. This could be achieved by utilizing differently shaped DNA origami structures and matching patterns on the surface. Additional breaking of the C₃ symmetry of the equilateral triangular DNA origami structure enables not only spacial but also rotational control.^[12] Thus the method demonstrated here has the potential to expand to a variety of optical applications that rely on complex surface patterning such as wave-guiding and optical circuitry self-assembled from colloidal particles.

Supporting Information

Supporting Information is available from the Wiley Online Library or from the author.

Acknowledgements

The authors thank Philip Altpeter and Christian Obermayer for assistance in the cleanroom specifically with EBL. Besides all the group members, the authors thank Susanne Kempfer for the help in the laboratory. C.S., I.V.M., and T.L. acknowledge funding from the ERC consolidator grant ‘DNA Funs’ (Project ID: 818635). T.L. further acknowledge support from the cluster of excellence e-conversion EXC 2089/1-390776260.

Open access funding enabled and organized by Projekt DEAL.

Conflict of Interest

The authors declare no conflict of interest.

Data Availability Statement

The data that support the findings of this study are available in the supplementary material of this article.

Keywords

dna origami, metasurface, nanolithography, nanoparticles, nanostructures, plasmonics, surface patterning

Received: March 19, 2024
Published online: May 10, 2024

- [1] W. T. Chen, A. Y. Zhu, V. Sanjeev, M. Khorasaninejad, Z. Shi, E. Lee, F. Capasso, *Nat. Nanotechnol.* **2018**, *13*, 220.
- [2] W. Zhao, H. Jiang, B. Liu, J. Song, Y. Jiang, C. Tang, J. Li, *Sci. Rep.* **2016**, *6*, 30613.
- [3] L. Caspani, R. P. M. Kaipurath, M. Clerici, M. Ferrera, T. Roger, J. Kim, N. Kinsey, M. Pietrzyk, A. Di Falco, V. M. Shalaev, A. Boltasseva, D. Faccio, *Phys. Rev. Lett.* **2016**, *116*, 233901.
- [4] B. Shen, V. Linko, K. Tapio, S. Pikker, T. Lemma, A. Gopinath, K. V. Gothelf, M. A. Kostianen, J. J. Toppari, *Sci. Adv.* **2018**, *4*, eaap8978.
- [5] C. T. Diagne, C. Brun, D. Gasparutto, X. Baillin, R. Tiron, *ACS Nano* **2016**, *10*, 6458.
- [6] S. P. Surwade, F. Zhou, B. Wei, W. Sun, A. Powell, C. O'Donnell, P. Yin, H. Liu, *J. Am. Chem. Soc.* **2013**, *135*, 6778.
- [7] C. Tian, H. Kim, W. Sun, Y. Kim, P. Yin, H. Liu, *ACS Nano* **2017**, *11*, 227.
- [8] G. Thomas, C. T. Diagne, X. Baillin, T. Chevolleau, T. Charvolin, R. Tiron, *ACS Appl. Mater. Interfaces* **2020**, *12*, 36799.
- [9] A. M. Hung, C. M. Micheel, L. D. Bozano, L. W. Osterbur, G. M. Wallraff, J. N. Cha, *Nat. Nanotechnol.* **2010**, *5*, 121.
- [10] S. P. Surwade, S. Zhao, H. Liu, *J. Am. Chem. Soc.* **2011**, *133*, 11868.
- [11] Z. Jin, W. Sun, Y. Ke, C.-J. Shih, G. L. Paulus, Q. Hua Wang, B. Mu, P. Yin, M. S. Strano, *Nat. Commun.* **2013**, *4*, 1663.
- [12] A. Gopinath, C. Thachuk, A. Mitskovets, H. A. Atwater, D. Kirkpatrick, P. W. K. Rothmund, *Science* **2021**, *371*, eabd6179.
- [13] D. Huang, K. Patel, S. Perez-Garrido, J. F. Marshall, M. Palma, *ACS Nano* **2019**, *13*, 728.
- [14] A. Gopinath, E. Miyazono, A. Faraon, P. W. K. Rothmund, *Nature* **2016**, *535*, 401.
- [15] S. M. Douglas, H. Dietz, T. Liedl, B. Högberg, F. Graf, W. M. Shih, *Nature* **2009**, *459*, 414.
- [16] P. W. K. Rothmund, *Nature* **2006**, *440*, 297.
- [17] S. M. Douglas, A. H. Marblestone, S. Teerapittayanon, A. Vazquez, G. M. Church, W. M. Shih, *Nucleic Acids Res.* **2009**, *37*, 5001.
- [18] B. Shen, M. A. Kostianen, V. Linko, *Langmuir* **2018**, *34*, 14911.
- [19] C. Hartl, K. Frank, H. Amenitsch, S. Fischer, T. Liedl, B. Nickel, *Nano Lett.* **2018**, *18*, 42609.
- [20] J. J. Funke, H. Dietz, *Nat. Nanotechnol.* **2016**, *11*, 147.
- [21] C. Chen, X. Wei, M. F. Parsons, J. Guo, J. L. Banal, Y. Zhao, M. N. Scott, G. S. Schlau-Cohen, R. Hernandez, M. Bathe, *Nat. Commun.* **2022**, *13*, 4935.
- [22] A. Kuzyk, R. Schreiber, Z. Fan, G. Pardatscher, E.-M. Roller, A. Högele, F. C. Simmel, A. O. Govorov, T. Liedl, *Nature* **2012**, *483*, 311.
- [23] R. J. Kershner, L. D. Bozano, C. M. Micheel, A. M. Hung, A. R. Fornof, J. N. Cha, C. T. Rettner, M. Bersani, J. Frommer, P. W. K. Rothmund, G. M. Wallraff, *Nat. Nanotechnol.* **2009**, *4*, 557.
- [24] A. Gopinath, P. W. K. Rothmund, *ACS Nano* **2014**, *8*, 12030.
- [25] P. Piskunen, B. Shen, A. Keller, J. J. Toppari, M. A. Kostianen, V. Linko, *ACS Appl. Nano Mater.* **2021**, *4*, 529.
- [26] B. Shen, V. Linko, K. Tapio, M. A. Kostianen, J. J. Toppari, *Nanoscale* **2015**, *7*, 11267.
- [27] W. Rechberger, A. Hohenau, A. Leitner, J. Krenn, B. Lamprecht, F. Aussenegg, *Opt. Commun.* **2003**, *220*, 137.
- [28] C. Lin, S. D. Perrault, M. Kwak, F. Graf, W. M. Shih, *Nucleic Acids Res.* **2013**, *41*, e40.

- [29] I. V. Martynenko, E. Erber, V. Ruider, M. Dass, G. Posnjak, X. Yin, P. Altpeter, T. Liedl, *Nat. Nanotechnol.* **2023**.
- [30] X. Liu, F. Zhang, X. Jing, M. Pan, P. Liu, W. Li, B. Zhu, J. Li, H. Chen, L. Wang, J. Lin, Y. Liu, D. Zhao, H. Yan, C. Fan, *Nature* **2018**, 559, 593.
- [31] M. Pachitariu, C. Stringer, *Nat. Methods* **2022**, 19, 1634.
- [32] T. Kraus, L. Malaquin, H. Schmid, W. Riess, N. D. Spencer, H. Wolf, *Nat. Nanotechnol.* **2007**, 2, 570.
- [33] A. S. Urban, A. A. Lutich, F. D. Stefani, J. Feldmann, *Nano Lett.* **2010**, 10, 4794.
- [34] J. Do, M. Fedoruk, F. Jäckel, J. Feldmann, *Nano Lett.* **2013**, 13, 4164.